Second feature of the matter two-point function

Vittorio Tansella*

Département de Physique Théorique and Center for Astroparticle Physics, Université de Genève, 24 quai Ansermet, CH–1211 Genève 4, Switzerland

(Received 24 April 2018; published 21 May 2018)

We point out the existence of a second feature in the matter two-point function, besides the acoustic peak, due to the baryon-baryon correlation in the early Universe and positioned at twice the distance of the peak. We discuss how the existence of this feature is implied by the well-known heuristic argument that explains the baryon bump in the correlation function. A standard χ^2 analysis to estimate the detection significance of the second feature is mimicked. We conclude that, for realistic values of the baryon density, a SKA-like galaxy survey will not be able to detect this feature with standard correlation function analysis.

DOI: 10.1103/PhysRevD.97.103520

I. INTRODUCTION

One of the most important probes of the large-scale structures (LSS) of the Universe is the two-point function of galaxies. Measurements of the two-point function (2 pF) have been reported by different collaborations [1–6] and, in the future, upcoming redshift surveys will probe the LSS of the Universe at deeper redshift and for larger volumes [7,8], with unprecedented precision.

With these surveys, we can nicely link late-time measurements to early-time physics. The most striking example are the acoustic oscillations in the primordial plasma—first predicted in [9–11]—which leave their imprint in cosmological observables. Their measurement is considered as one of the most important successes of the ΛCDM model. In the cosmic microwave background, the scale of the baryon acoustic oscillations (BAO) is a probe of the sound horizon at decoupling and it manifests itself as a series of peaks in the angular spectrum [12]. A similar feature can also be seen in the matter power spectrum [13], while, in the 2 pF, the same physics is responsible for a single peak located at a comoving distance slightly bigger—as we will explain in Sec. II—than the sound horizon at decoupling.

The BAO peak in the correlation function has been first measured in [14]. Since then it has been systematically used as a standard ruler to probe the distance-redshift relation [15–17], in order to constrain the cosmic expansion history [18]. The peak is also sensitive to other cosmological parameters [19–21]. A complication arises as the position of the peak measured with data cannot be fitted with linear theory: non-linearities affect both the position and the shape of the BAO feature [22–27].

Here we consider a second feature: a trough in the correlation function positioned at twice the distance of the peak. The existence of this feature is implied by the well-known heuristic argument that is commonly used to explain the BAO peak (see Sec. II), but rarely mentioned in the literature. In Sec. III, we mimic the fitting procedure—used by galaxy surveys to measure the peak position—to study the expected detection significance of the second feature for an SKA-like survey.

II. THE SECOND FEATURE

We outline, in this section, the heuristic argument given in the seminal paper [22] and summarized in the review [28]. This will give us insight on how this argument implies a second feature in the correlation function. The technical foundations can be found in [29–31].

Let us focus on some initial overdense point in the primordial plasma—when baryons are tightly coupled to photons via Thomson scattering. If the fluctuations are adiabatic, the overdensity will be shared by all species: in particular a region overdense in photons will also have an overpressure with respect to its surroundings. This pressure imbalance causes an acoustic wave in the baryon-photon plasma which travels at the speed of sound c_s until baryons decouple from the photons. When this happens the baryon's speed of sound goes to zero and the wave is frozen: the initial overdensity is now composed only of dark matter while baryons have created an overdense spherical region around the initial point. Every overdensity will behave as we just described and the net result is that matter is more likely to cluster with a correlation length corresponding to the sound horizon at decoupling. It is clear that this process, as we have already anticipated, is responsible for the BAO peak: the correlation function is defined as the excess probability (over Poisson noise) of finding two tracers separated by a comoving distance s and hence it peaks for $s \sim s_{\rm hor}$, where the comoving sound horizon is defined as

*vittorio.tansella@unige.ch

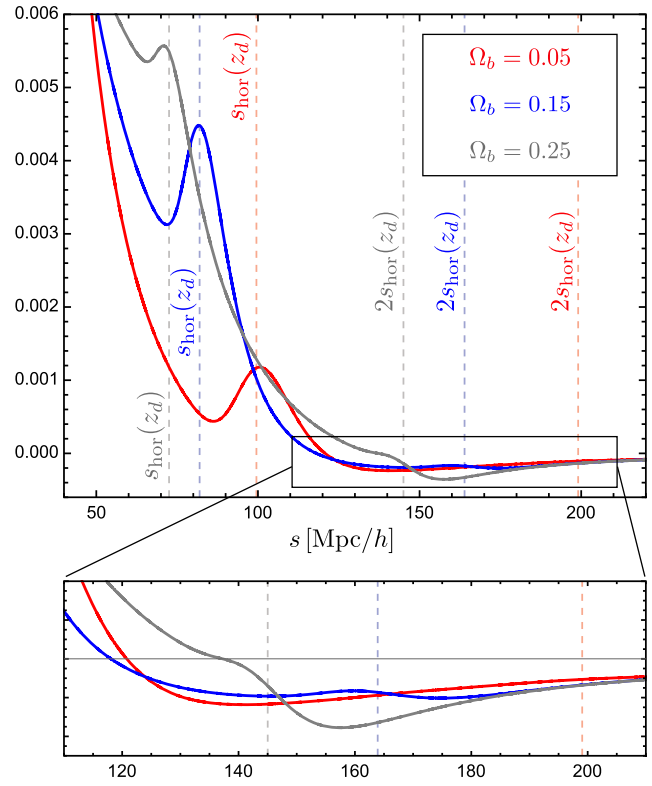

FIG. 1. The angle-averaged matter correlation function at $\bar{z} = 1$ for three different cosmologies with $\Omega_b = 0.25$ (gray), $\Omega_b = 0.15$ (blue) and $\Omega_b = 0.05$ (red). The total matter density is fixed to $\Omega_m = 0.31$ and the sound horizon at the drag epoch for the different models is shown.

$$s_{\mathrm{hor}} = \int_0^{t_{\mathrm{drag}}} dt c_s(t)(1+z). \tag{1}$$

and t is cosmic time. The end of the Compton drag epoch t_{drag} is the time at which the baryons are released from the drag of photons (at a later time than photon-decoupling, roughly at $z_{\mathrm{drag}} \sim 1000$). It is the moment at which the baryons' velocity decouples from the photons. If we go back to our idealistic picture of a dark matter perturbation surrounded by a spherical shell of baryons we see that the correlation will not only be enhanced at s_{hor} but, as all the baryons are in the shell, we will also get a trough when the correlation length reaches the diameter of the shell: $2s_{\mathrm{hor}}$. In other words—in our idealized picture—as long as the correlation length is $< 2s_{\mathrm{hor}}$ the baryon-baryon correlation contributes to the matter 2 pF as it is always likely to "find" two baryons in the shell. On the other hand, when the correlation length reaches the diameter of the shell, the baryon-baryon contribution has a sharp trough. This second feature (2 FT) is illustrated in Fig. 1: we can clearly see the drop in the 2 pF at $2s_{\mathrm{hor}}$ for high values of Ω_b, while the feature is less pronounced when baryons contribute less to the energy-density budget.

One might notice that, even in linear theory, the position of the acoustic peak is not exactly centered on s_{hor}: this is a known effect due to imperfect baryon-photon coupling, which allows photons to diffuse out of the perturbation and drag the baryons with them,[1] and velocity overshoot—both discussed in detail in [32]. Note that the dark matter overdensity does not remain at the center of the shell as it is gravitationally bound to the outgoing species, this does however not change the position of the peak. Despite these complications the peak is an extremely interesting cosmological observable as it is sensitive to a range of cosmological parameters. For example s_{hor} is directly related to the sound speed c_s via Eq. (1) which, in turn, is related to the Ω_b and Ω_γ ratio. The positions of the features are also sensitive to the expansion history prior to decoupling as the propagation time of the sound wave depends on the expansion rate, introducing for example a subtle dependence on Ω_ν (see [33] for a comprehensive treatment). Finally, measuring the positions of the features as a function of redshift—using them as statistical standard rulers—constrains the late-time expansion rate and gives information on Ω_m, Ω_Λ and the equation of state of dark energy w.

We could naively think that, since we are searching for a feature at twice the separation of the BAO peak, we are safe from nonlinear effects at these very large scales. This is only partially correct. Nonlinear effects on the BAO peak come in two aspects: a broadening of the feature and a shift of the peak position. The damping effect is easily understood in real space, where nonlinear physics can move the tracers around, on the scale of ∼10 Mpc, pulling them out of the 100 Mpc$/h$ shell and hence broadening the peak feature [25]. In Fourier space, this effect is responsible for the smoothing of the subsequent peaks in the power spectrum (see e.g. [34]). The fact that we are looking at two galaxies at a distance where linear physics should give an adequate description is not important in this case: the local nonlinearities around the two tracers have an observable (and important) effect. For this reason we expect the 2FT to suffer from the same nonlinear correction to its shape as it is not protected from nonlinear broadening. We stick to the linear description of the 2 pF in this work where the feature is sharper and therefore we will overestimate the detection significance in Sec. III. This does not change our conclusions. On the other hand, in order to induce a shift in the position of the feature, nonlinear physics has to coherently and systematically move tracers separated by s_{hor} or $2s_{\mathrm{hor}}$ either closer or further away from each other. The small shift of the BAO peak has been widely investigated [24,27,35–38] and in this sense the fact the 2FT is located at larger scales means it will be less affected, as the

[1]In Fourier and angular space, this effect is responsible for the *"Silk damping."*

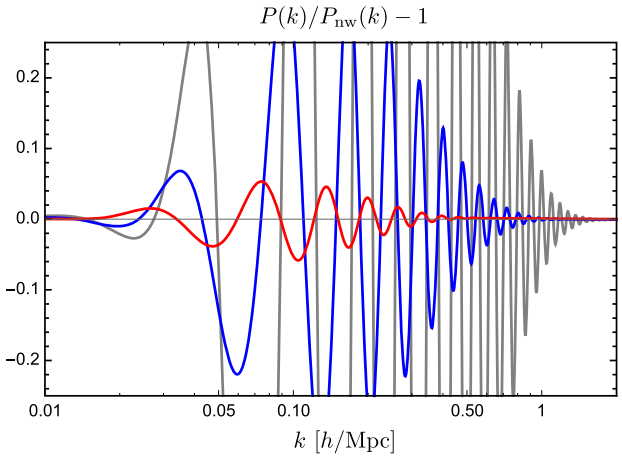

FIG. 2. The residual BAO oscillations $P(k)/P_{\rm nw}(k)-1$ once the broadband shape is factored out with the no-wiggle power spectrum $P_{\rm nw}$, defined in Eq. (13). Color coding as in Fig. 1.

position is only sensible to nonlinear effects at the ∼200 Mpc/h scale.

A. Fourier space

Let us now discuss how the simple picture depicted in this section is translated in Fourier space.[2] The matter transfer function can be written as

$$T_m(k) = f_{\rm cdm}T_{\rm cdm}(k) + f_b T_b(k), \tag{2}$$

where $f_{\rm cdm} = \Omega_{\rm cdm}/\Omega_m$, $f_b = \Omega_b/\Omega_m$, and we drop the redshift dependence here. $T_{\rm cdm}$ is the smooth contribution of cold dark matter to the transfer function while $T_b \sim \sin(s_{\rm hor}k)$ contains the "sine-wave" oscillations of the BAO. The power spectrum is then proportional to

$$k^3P(k) \sim f_{\rm cdm}^2T_{\rm cdm}^2 + 2f_{\rm cdm}f_bT_{\rm cdm}T_b + f_b^2T_b^2. \tag{3}$$

For $f_b \ll f_{\rm cdm}$ the last term is subdominant and $P(k)$ has the familiar shape of a superposition of a smooth function and a "sine-wave." On the other hand for $f_b \gtrsim f_{\rm cdm}$ the squared oscillations start to dominate, increasing both the frequency of the BAO and their amplitude (see Fig. 2). When we Fourier transform to obtain the 2 pF, the "sine-wave" part of $P(k)$ contributes to the BAO peak while the "sine-square" part from T_b^2 is responsible for the feature at twice the peak distance as it oscillates with twice the frequency. Hence, also in Fourier space, bigger values of f_b correspond to a more pronounced 2FT.

[2]This argument is discussed in https://www.cfa.harvard.edu/~deisenst/acousticpeak/spherical_acoustic.pdf: a short but vey nice essay which, to our knowledge, is the only place where the 2FT is briefly mentioned for the purely baryonic case.

III. FITTING METHODOLOGY

We now want to gain insight on the ability of galaxy surveys to detect the second feature in the matter two-point function. The procedure to detect the BAO peak is now well established (as described in [39] and used e.g. in [40]) and we follow it here for the 2FT. The BAO detection is usually quoted as the χ^2 difference between the best-fit model and the model with no features. In other words we study how reliably we can reject a no-feature model. We do not deal with real data here but generate a fake "data" vector $\boldsymbol{\xi}$ from our fiducial model and compute the χ^2 from the standard definition

$$\chi^2_{\rm fit}(\alpha) = (\boldsymbol{\xi}_{\rm fit}(\alpha) - \boldsymbol{\xi})\ {}^{\rm T}\mathbf{C}^{-1}(\boldsymbol{\xi}_{\rm fit}(\alpha) - \boldsymbol{\xi}), \tag{4}$$

where $\mathbf{C}$ is the covariance matrix for the fiducial model, defined in Appendix A. The quantity α is the scale dilatation parameter which measures the position of the feature (being the BAO peak or the 2FT) with respect to the fiducial model. In real data analyses, α is a measure of

$$\alpha = \frac{D_V(z)s_{*,\rm fid}}{D_V^{\rm fid}(z)s_*} \tag{5}$$

where the subscript 'fid' means 'fiducial', s_* is the comoving position of the feature and D_V is the spherically averaged[3] distance defined as

$$D_V(z) = [cz(1+z)D_A^2(z)\mathcal{H}(z)]^{1/3}. \tag{6}$$

The parameter α is the measurement of the 2FT scale in the sense that it characterizes any observed shift in the relative position of the acoustic feature in the data versus the model. The value of α which minimizes χ^2 is related to the feature position via Eq. (5), and the feature position roughly marks $2s_{\rm hor}$.

In this work the fiducial model is generated starting from the linear matter power spectrum $P(k)$ obtained from CLASS [41] (multiplied by the large-scale galaxy bias $b^2(z)$ given in Appendix A) and converted into the full-sky correlation function [42] using the COFF-E [43] code.[4] To mimic most BAO analyses we include the effect of redshift-space distortion in the 2 pF but neglect other relativistic effects (such as lensing and the Doppler effect). We also neglect nonlinear damping[5] and set the streaming scale to zero as

[3]Note that in real data situations both the angle averaged parameter α and an additional parameter ϵ are considered: ϵ parametrizes the anisotropic clustering due to redshift-space distortions and due to an analysis where an incorrect cosmology is assumed.

[4]Available soon at https://github.com/JCGoran/coffe.

[5]We also do not consider a Gaussian damping term which is commonly introduced in the Fourier transform $P(k) \to \xi(s)$ to improve numerical convergence as the COFF-E code is based on the very reliable 2-FAST algorithm [44].

our fiducial model—from which we draw data—is fully linear. To improve the signal-to-noise, galaxy surveys measure the spherically averaged two-point function $\xi_0(s)$ (the monopole) and the quadrupole $\xi_2(s)$ defined as

$$\xi_\ell(s) = \frac{2\ell+1}{2}\int d\mu \xi(s,\mu)\mathcal{P}_\ell(\mu), \tag{7}$$

where $\mathcal{P}_\ell$ is the Legendre polynomial of degree ℓ and μ is the orientation with respect to the line of sight at which we measure the 2 pF. Our data vector is then given by

$$\boldsymbol{\xi} = \begin{pmatrix} \boldsymbol{\xi}_0 \\ \boldsymbol{\xi}_2 \end{pmatrix}. \tag{8}$$

Fake "data" are generated for three different cosmologies: the fiducial *Planck2015*[6] cosmology and two unrealistic toy models with $\Omega_b = 0.25$ and $\Omega_b = 0.15$—keeping Ω_m and all the other parameters fixed—to illustrate the procedure in models where the 2FT is more pronounced. The binning of the data vectors ($\boldsymbol{\xi}_0$ and $\boldsymbol{\xi}_2$) is chosen in a range of $\sim$75 Mpc$/h$ around the value $2s_{\rm hor}$ for each fiducial model and with a bin size $L_p = 3$ Mpc$/h$, for 25 bins in total. The covariance matrix is computed for an SKA-like survey, with parameters given in Appendix A.

A. Fitting models

To fit the correlation function we adopt two template models, one with the BAO peak and the 2FT and the other with no baryonic features. The fit is performed, as in recent BAO data analyses, with five parameters: a multiplicative bias B, the scale dilatation α and (as we are only interested in the position of the 2FT) a second-order polynomial to marginalize over the broad-band shape of the multipoles. We then write

$$\begin{aligned} \xi_0^{\rm fit}(s) &= B^2\xi_0^{\rm mod}(\alpha, s) + A_0(s), \\ \xi_2^{\rm fit}(s) &= \xi_2^{\rm mod}(\alpha, s) + A_2(s), \end{aligned} \tag{9}$$

where we define

$$A_\ell(s) = \frac{a_{1,\ell}}{s^2} + \frac{a_{2,\ell}}{s} + a_{\ell,3}; \quad \ell = 0, 2, \tag{10}$$

with three nuisance parameters per multipole (a_1, a_2, a_3), to account for the overall unknown shape of the correlation function. A difference with the standard approach is that we set here $B = 1$ for two reasons. Firstly, as we are not dealing with real data, we have full control on the linear bias parameter when we generate fake data from our fiducial model. Secondly we are not comparing different cosmologies (for which the amplitude of the feature might change) but the same cosmology with and without the feature. This also prevents the data to be fitted only by the quadratic polynomial A_ℓ.

The first template model is simply given by

$$\xi_\ell^{\rm mod}(\alpha, s) = \xi_\ell^{\rm fid}(\alpha s). \tag{11}$$

Note that when performing the BAO analysis in real space, it is standard practice to shift the all model as in Eq. (11). A different approach is usually employed in the Fourier space analysis where only the BAO oscillations are shifted. As the nuisance parameters $a_{i,\ell}$ are marginalizing over the broad-band shape of the multipoles, this has no effect [45].

The second template is the "de-wiggled" model. It is a phenomenological prescription widely used in BAO analysis: it consists in generating a correlation function starting from a power spectrum $P_{\rm nw}(k)$ in which the BAO features have been erased. To obtain $P_{\rm nw}(k)$ we start with the Eisenstein and Hu [46,47] approximated power spectrum $P_{\rm EH}(k)$ and perform a Gaussian smoothing on the ratio $P(k)/P_{\rm EH}(k)$:

$$P_{\rm nw}(k) = P_{\rm EH}(k)\mathcal{S}[P(k)/P_{\rm EH}(k)], \tag{12}$$

where $\mathcal{S}$ schematically represents the smoothing. The no-wiggle spectrum is then given by [26]

$$\begin{aligned} \frac{P_{\rm nw}(10^{k_{\log}})}{P_{\rm EH}(10^{k_{\log}})} = \frac{1}{\sqrt{2\pi}\lambda}\int dq_{\log}\Bigg[\frac{P(10^{q_{\log}})}{P_{\rm EH}(10^{q_{\log}})} \\ \times \exp\left(-\frac{1}{2\lambda^2}(k_{\log} - q_{\log})^2\right)\Bigg], \end{aligned} \tag{13}$$

where λ is a parameter that controls the size of the smoothing. We found the best results for $\lambda = 0.14$ Mpc$/h$. In Fig. 2, we plot the fractional difference of the no-wiggle power spectrum and the linear one. The multipoles of the correlation function with no feature $\xi_\ell^{\rm nw}(s)$ are then generated by feeding COFF-E with $P_{\rm nw}$ and the second template model is given by

$$\xi_\ell^{\rm mod}(\alpha, s) = \xi_\ell^{\rm nw}(\alpha s). \tag{14}$$

For every value of α we fit the remaining parameters to minimize the χ^2 for both models. We chose only one fiducial redshift $z = 1$, hence we require the size of the redshifts bin of the survey to be $\Delta z \gtrsim 0.2$. We focus here only on one redshift bin as the shape of the correlation function is nearly constant at large scales for the depth accessible by galaxy surveys and the analysis is trivially extended to more bins, given also the fact that we can treat them as uncorrelated to a good approximation. In Fig. 3, we show the fiducial model monopole $\xi_0^{\rm fid}(s)$ with the error bars obtained from Eq. (A8), together with the best-fit no-feature model of Eq. (14). Clearly as Ω_b decreases the

[6]We set $h = 0.676$, $\Omega_{\rm cdm} = 0.26$, $\Omega_b = 0.048$, $\Omega_\Lambda = 0.68$. The primordial spectrum has $n_s = 0.96$ and $A_s = 2.22 \times 10^{-9}$ at $k_{\rm pivot} = 0.05$ Mpc^{-1}.

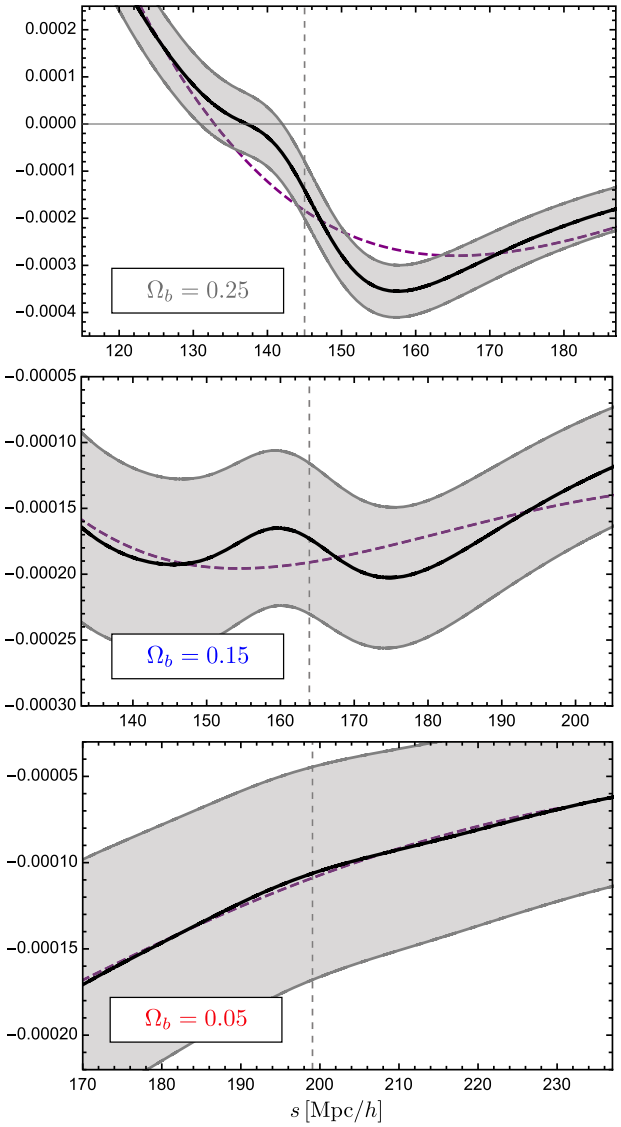

FIG. 3. A zoom of Fig. 1 for the range used in the $\Delta\chi^2$ estimation, where the second feature is clearly visible for high-baryon models. The gray region marks the error bars given by the covariance for an SKA-like survey and the purple dashed line is the best-fit non-BAO (de-wiggled) model.

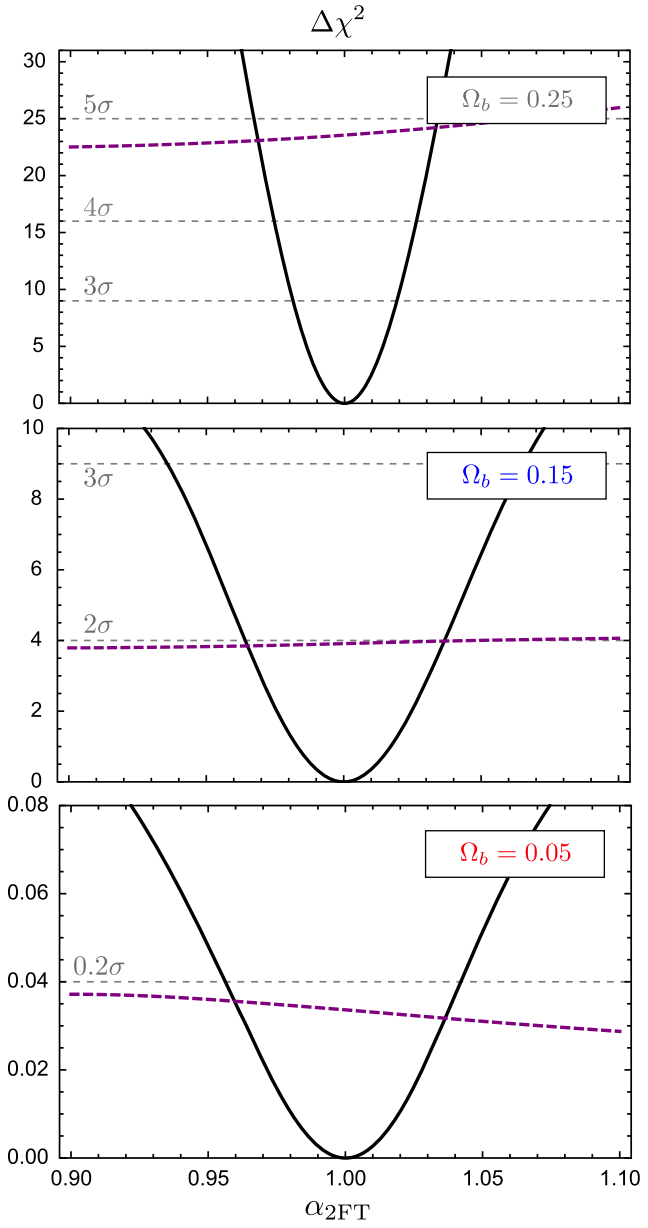

FIG. 4. The $\Delta\chi^2(\alpha) = \chi^2(\alpha) - \chi^2_{\mathrm{min}}$ as a function of the BAO-parameter $\alpha_{2\,\mathrm{FT}}$. The solid line is the model of Eq. (11) while the dashed curve displays the same information for a no BAO model (Eq. (14)), where $\Delta\chi^2$ is determined by subtracting the minimum χ^2_{min} from the BAO model.

feature is less and less pronounced and the no-feature model is an increasingly better fit to the data. For a realistic model with $\Omega_b \simeq 0.05$ the 2FT is barely visible and lies completely within the error bars. This situation is reflected when we compare the $\Delta\chi^2(\alpha) = \chi^2(\alpha) - \chi^2_{\mathrm{min}}$ for the two templates. We can read off the detection significance for the 2FT in Fig. 4. In the two toy models—with an unrealistically high baryon fraction—the no-feature templates are disfavored at $\sim 5\sigma$ and $\sim 2\sigma$ respectively. The realistic model *Planck2015* shows no preference for the template which correctly describes the 2FT compared to the smoothed template. We have checked that these results marginally change when we vary the order of the polynomial fit in Eq. (10). Note that the no-BAO model has a broad χ^2 as the lack of features makes the scale less constrainable.

IV. CONCLUSIONS

In this work, we have introduced a second feature in the matter correlation function. This feature, positioned at twice the distance of the BAO peak, is understood—in the early Universe—as a trough in the baryon-baryon correlation for separations bigger than twice the sound horizon at t_{drag}. The feature is clearly visible in models with

a high baryon fraction but in a realistic cosmological model it is a very small effect. We proved this with a χ^2 analysis that showed how—in an SKA-like survey—it is not possible to distinguish between the models with and without the feature. We have considered only one redshift bin and it is possible to increase the detection significance by a factor $\sim\sqrt{N}$ by considering N bins; however, the analysis requires $\Delta z_{\rm bin} \gtrsim 0.2$ hence limiting the number of bins N in which we can split a galaxy catalog. Furthermore, the fact that at $2s_{\rm hor}$ the error is cosmic variance dominated suggests that the two-point function is not the best observable to detect this feature.

In a Fourier space analysis, the effect described here is correctly modeled if the template $P(k)$ is generated from a Boltzmann code such as CLASS [41,48] or CAMB [49].

It is nevertheless interesting to study if other observable —e.g. intensity mapping—are more sensitive to this feature which, if detected, would provide an additional probe for early-time cosmology. We leave this matter for future work.

ACKNOWLEDGMENTS

We wish to thank Jonathan Blazek, Enea Di Dio, Ruth Durrer, Fabien Lacasa, Martin Kunz, and Elena Sellentin for useful discussions. We additionally acknowledge useful comments on the draft of this paper from Ruth Durrer, Martin Kunz, and Davide Racco. The author acknowledges support by the Swiss National Science Foundation.

APPENDIX: COVARIANCE MATRIX

The simplest estimator we can construct for the multipoles is given in [43] as

$$\hat{\xi}_\ell(x) = \frac{2\ell+1}{4\pi}\frac{L_p^5}{x^2 V}\sum_{ij}\Delta_i\Delta_j\mathcal{P}_\ell(\mu_{ij})\delta_K(x_{ij}-x),$$

and the covariance matrix is defined by

$$\mathrm{cov}^{(\xi)}_{\ell\ell'}(x_i,x_j) \equiv \langle\hat{\xi}_\ell(x_i)\hat{\xi}_{\ell'}(x_j)\rangle - \langle\hat{\xi}_\ell(x_i)\rangle\langle\hat{\xi}_{\ell'}(x_j)\rangle.$$

The variance of the number counts has two contributions

$$\langle\Delta_i\Delta_j\rangle = \frac{1}{d\bar{N}}\delta_{ij} + C_{ij}. \tag{A1}$$

The first term, where $d\bar{N}$ is the average number of tracers per pixel, accounts for shot noise, coming from the fact that we are Poisson sampling from the underlying density distribution and it is a contribution to the correlation at zero separation. The second term is the cosmic variance contribution. For simplicity we perform the covariance calculation in the flat-sky approximation where the 2 pF is simply written

$$\xi(\bar{z},s,\mu)_{\rm flat-sky} = \frac{D_1^2(\bar{z})}{D_1^2(0)}[c_0(\bar{z})I_0^0(s) - c_2(\bar{z})I_2^0(s)\mathcal{P}_2(\mu) + c_4(\bar{z})I_4^0(s)\mathcal{P}_4(\mu)], \tag{A2}$$

with

$$c_0 = b^2 + \frac{2}{3}bf + \frac{f^2}{5}, \tag{A3}$$

$$c_2 = \frac{4}{3}bf + \frac{4}{7}f^2, \tag{A4}$$

$$c_4 = \frac{8}{35}f^2. \tag{A5}$$

Here $D_1(\bar{z})$ is the growth factor,

$$f(\bar{z}) = \frac{d\ln D_1}{d\ln(a)} \tag{A6}$$

is the growth rate and we have also introduced the integrals

$$I_\ell^n(s) = \int\frac{dkk^2}{2\pi^2}P(k)|_{z=0}\frac{j_\ell(ks)}{(ks)^n}. \tag{A7}$$

Assuming Gaussianity (i.e. we write four-point functions as products of two-point functions), we follow the procedure outlined in [43,50] and obtain

$$\mathrm{cov}^{(\xi)}_{\ell\ell'}(x_i,x_j) = \frac{i^{\ell-\ell'}}{V}\left[\frac{2\ell+1}{2\pi\bar{n}^2L_p x_i^2}\delta_{ij}\delta_{\ell\ell'} + \frac{1}{\bar{n}}\mathcal{G}_{\ell\ell'}(x_i,x_j)\sum_\sigma c_\sigma\begin{pmatrix}\ell & \ell' & \sigma\\ 0 & 0 & 0\end{pmatrix}^2 + \mathcal{D}_{\ell\ell'}(x_i,x_j)\sum_\sigma\tilde{c}_\sigma\begin{pmatrix}\ell & \ell' & \sigma\\ 0 & 0 & 0\end{pmatrix}^2\right], \tag{A8}$$

where $\bar{n}$ is the mean number density in the redshift bin and we have defined

$$\mathcal{G}_{\ell\ell'}(x_i,x_j) = 2w(\ell,\ell')\int dkk^2P(k,\bar{z})j_\ell(kx_i)j_{\ell'}(kx_j),$$

$$\mathcal{D}_{\ell\ell'}(x_i,x_j) = w(\ell,\ell')\int dkk^2P^2(k,\bar{z})j_\ell(kx_i)j_{\ell'}(kx_j),$$

with

$$w(\ell,\ell') = \frac{(2\ell+1)(2\ell'+1)}{\pi^2}, \tag{A9}$$

and the modified redshift-distortion coefficients

$$\tilde{c}_0 = c_0^2 + \frac{c_2^2}{5} + \frac{c_4^2}{9}, \tag{A10}$$

$$\tilde{c}_2 = \frac{2}{7}c_2(7c_0 + c_2) + \frac{4}{7}c_2c_4 + \frac{100}{693}c_4^2, \tag{A11}$$

$$\tilde{c}_4 = \frac{18}{35}c_2^2 + 2c_0c_4 + \frac{40}{77}c_2c_4 + \frac{162}{1001}c_4^2, \tag{A12}$$

$$\tilde{c}_6 = \frac{10}{99}c_4(9c_2 + 2c_4), \tag{A13}$$

$$\tilde{c}_8 = \frac{490}{1287}c_4^2. \tag{A14}$$

The covariance matrix $\mathbf{C}$ in Eq. (4) is then written as

$$\mathbf{C} = \begin{pmatrix} \mathbf{cov}_{00} & \mathbf{cov}_{02} \\ \mathbf{cov}_{20} & \mathbf{cov}_{22} \end{pmatrix}, \tag{A15}$$

where $\mathbf{cov}_{\ell\ell',ij} = \mathrm{cov}^{(\xi)}_{\ell\ell'}(x_i, x_j)$.

For a SKA-like survey the parameters are taken from [51] (Table III). We consider a single redshift-bin centered at $\bar{z} = 1$ with thickness $\Delta z = 0.2$, sky coverage $f_{\rm sky} \simeq 0.72$, mean number density $\bar{n} \simeq 8.7 \times 10^{-4}$ Mpc^{-3} and bias $b \simeq 1.3$.

[1] D. H. Jones *et al.*, The 6dF galaxy survey: Final redshift release (DR3) and southern large-scale structures, Mon. Not. R. Astron. Soc. **399**, 683 (2009).

[2] D. Parkinson *et al.*, The WiggleZ Dark Energy Survey: Final data release and cosmological results, Phys. Rev. D **86**, 103518 (2012).

[3] S. Alam, F. D. Albareti, C. Allende Prieto, F. Anders, S. F. Anderson, T. Anderton, B. H. Andrews, E. Armengaud, É. Aubourg, S. Bailey *et al.*, The eleventh and twelfth data releases of the sloan digital sky survey: Final data from SDSS-III, Astrophys. J. Suppl. Ser. **219**, 12 (2015).

[4] S. R. Hinton *et al.*, Measuring the 2D Baryon Acoustic Oscillation signal of galaxies in WiggleZ: Cosmological constraints, Mon. Not. R. Astron. Soc. **464**, 4807 (2017).

[5] M. Ata *et al.*, The clustering of the SDSS-IV extended Baryon Oscillation Spectroscopic Survey DR14 quasar sample: First measurement of baryon acoustic oscillations between redshift 0.8 and 2.2, Mon. Not. R. Astron. Soc. **473**, 4773 (2018).

[6] F. D. Albareti, C. Allende Prieto, A. Almeida, F. Anders, S. Anderson, B. H. Andrews, A. Aragón-Salamanca, M. Argudo-Fernández, E. Armengaud, E. Aubourg *et al.*, The 13th data release of the sloan digital sky survey: First spectroscopic data from the SDSS-IV survey mapping nearby galaxies at apache point observatory, Astrophys. J. Suppl. Ser. **233**, 25 (2017).

[7] R. Laureijs, J. Amiaux, S. Arduini, J. Augueres, J. Brinchmann, R. Cole, M. Cropper, C. Dabin, L. Duvet, A. Ealet *et al.*, Euclid Definition Study Report, arXiv: 1110.3193.

[8] R. Maartens, F. B. Abdalla, M. Jarvis, M. G. Santos, and *SKA Cosmology SWG* Collaboration, Overview of cosmology with the SKA, *Proc. Sci.*, AASKA14 (2015) 016.

[9] R. A. Sunyaev and Ya. B. Zeldovich, The Interaction of matter and radiation in the hot model of the universe, Astrophys. Space Sci. **7**, 20 (1970).

[10] R. A. Sunyaev and Ya. B. Zeldovich, Small scale fluctuations of relic radiation, Astrophys. Space Sci. **7**, 3 (1970).

[11] P. J. E. Peebles and J. T. Yu, Primeval adiabatic perturbation in an expanding universe, Astrophys. J. **162**, 815 (1970).

[12] P. A. R. Ade *et al. Planck* Collaboration, Planck 2015 results. XIII. Cosmological parameters, Astron. Astrophys. **594**, A13 (2016).

[13] A. Meiksin, M. J. White, and J. A. Peacock, Baryonic signatures in large scale structure, Mon. Not. R. Astron. Soc. **304**, 851 (1999).

[14] D. J. Eisenstein *et al. SDSS* Collaboration, Detection of the baryon acoustic peak in the large-scale correlation function of SDSS luminous red galaxies, Astrophys. J. **633**, 560 (2005).

[15] F. Beutler, C. Blake, M. Colless, D. H. Jones, L. Staveley-Smith, L. Campbell, Q. Parker, W. Saunders, and F. Watson, The 6dF Galaxy Survey: Baryon acoustic oscillations and the local Hubble constant, Mon. Not. R. Astron. Soc. **416**, 3017 (2011).

[16] C. Blake *et al.*, The WiggleZ Dark Energy Survey: Mapping the distance-redshift relation with baryon acoustic oscillations, Mon. Not. R. Astron. Soc. **418**, 1707 (2011).

[17] L. Anderson *et al.*, The clustering of galaxies in the SDSS-III Baryon Oscillation Spectroscopic Survey: baryon acoustic oscillations in the Data Release 9 spectroscopic galaxy sample, Mon. Not. R. Astron. Soc. **427**, 3435 (2012).

[18] D. J. Eisenstein, W. Hu, and M. Tegmark, Cosmic complementarity: H(0) and Omega(m) from combining CMB experiments and redshift surveys, Astrophys. J. **504**, L57 (1998).

[19] M. P. van Daalen, B. M. B. Henriques, R. E. Angulo, and S. D. M. White, The galaxy correlation function as a constraint on galaxy formation physics, Mon. Not. R. Astron. Soc. **458**, 934 (2016).

[20] D. Baumann, D. Green, and M. Zaldarriaga, Phases of new physics in the BAO spectrum, J. Cosmol. Astropart. Phys. 11 (2017) 007.

[21] D. Baumann, F. Beutler, R. Flauger, D. Green, M. Vargas-Magaa, A. Slosar, B. Wallisch, and C. Yche, First measurement of neutrinos in the BAO spectrum, arXiv: 1803.10741.

[22] D. J. Eisenstein, H.-j. Seo, and M. J. White, On the robustness of the acoustic scale in the low-redshift clustering of matter, Astrophys. J. **664**, 660 (2007).
[23] M. Crocce and R. Scoccimarro, Nonlinear evolution of baryon acoustic oscillations, Phys. Rev. D **77**, 023533 (2008).
[24] R. E. Smith, R. Scoccimarro, and R. K. Sheth, Eppur Si Muove: On the motion of the acoustic peak in the correlation function, Phys. Rev. D **77**, 043525 (2008).
[25] N. McCullagh and A. S. Szalay, Nonlinear behavior of baryon acoustic oscillations in redshift space from the Zel'dovich approximation, Astrophys. J. **798**, 137 (2015).
[26] Z. Vlah, U. Seljak, M. Y. Chu, and Y. Feng, Perturbation theory, effective field theory, and oscillations in the power spectrum, J. Cosmol. Asropart. Phys. 03 (**2016**) 057.
[27] S. Anselmi, G. D. Starkman, and R. K. Sheth, Beating nonlinearities: Improving the Baryon Acoustic Oscillations with the linear point, Mon. Not. R. Astron. Soc. **455**, 2474 (2016).
[28] B. A. Bassett and R. Hlozek, Baryon acoustic oscillations, in *Dark Energy*, edited by P. Ruiz-Lapuente (Cambridge University Press, Cambridge, England, 2010).
[29] S. Bashinsky and E. Bertschinger, Position-Space Description of the Cosmic Microwave Background and Its Temperature Correlation Function, Phys. Rev. Lett. **87**, 081301 (2001).
[30] S. Bashinsky and E. Bertschinger, Dynamics of cosmological perturbations in position space, Phys. Rev. D **65**, 123008 (2002).
[31] F. Montanari and R. Durrer, An analytic approach to baryon acoustic oscillations, Phys. Rev. D **84**, 023522 (2011).
[32] A. G. Sanchez, C. M. Baugh, and R. Angulo, What is the best way to measure baryonic acoustic oscillations?, Mon. Not. R. Astron. Soc. **390**, 1470 (2008).
[33] K. Thepsuriya and A. Lewis, Accuracy of cosmological parameters using the baryon acoustic scale, J. Cosmol. Astropart. Phys. 01 (2015) 034.
[34] S. Anselmi and M. Pietroni, Nonlinear power spectrum from resummed perturbation theory: A leap beyond the BAO scale, J. Cosmol. Astropart. Phys. 12 (2012) 013.
[35] V. Desjacques, M. Crocce, R. Scoccimarro, and R. K. Sheth, Modeling scale-dependent bias on the baryonic acoustic scale with the statistics of peaks of Gaussian random fields, Phys. Rev. D **82**, 103529 (2010).
[36] T. Baldauf, M. Mirbabayi, M. Simonovic, and M. Zaldarriaga, Equivalence principle and the baryon acoustic peak, Phys. Rev. D **92**, 043514 (2015).
[37] A. Obuljen, F. Villaescusa-Navarro, E. Castorina, and M. Viel, Baryon acoustic oscillations reconstruction with pixels, J. Cosmol. Astropart. Phys. 09 (2017) 012.
[38] D. Blas, M. Garny, M. M. Ivanov, and S. Sibiryakov, Time-sliced perturbation theory II: Baryon acoustic oscillations and infrared resummation, J. Cosmol. Astropart. Phys. 07 (2016) 028.
[39] X. Xu, N. Padmanabhan, D. J. Eisenstein, K. T. Mehta, and A. J. Cuesta, A 2% distance to $z = 0.35$ by reconstructing baryon acoustic oscillations—II: Fitting techniques, Mon. Not. R. Astron. Soc. **427**, 2146 (2012).
[40] M. V. Magana *et al.*, SDSS-III Baryon Oscillation Spectroscopic Survey: Analysis of Potential Systematics in Fitting of Baryon Acoustic Feature, arXiv:1312.4996.
[41] D. Blas, J. Lesgourgues, and T. Tram, The Cosmic Linear Anisotropy Solving System (CLASS) II: Approximation schemes, J. Cosmol. Astropart. Phys. 07 (2011) 034.
[42] V. Tansella, C. Bonvin, R. Durrer, B. Ghosh, and E. Sellentin, The full-sky relativistic correlation function and power spectrum of galaxy number counts. Part I: theoretical aspects, J. Cosmol. Astropart. Phys. 03 (2018) 019.
[43] C. Bonvin, R. Durrer, G. Jelic-Cizmek, and V. Tansella, COFF-E: A code for the full-sky relativistic galaxy correlation function (to be published).
[44] H. S. Grasshorn Gebhardt and D. Jeong, Fast and accurate computation of projected two-point functions, Phys. Rev. D **97**, 023504 (2018).
[45] L. Anderson *et al. BOSS* Collaboration, The clustering of galaxies in the SDSS-III Baryon Oscillation Spectroscopic Survey: baryon acoustic oscillations in the Data Releases 10 and 11 Galaxy samples, Mon. Not. R. Astron. Soc. **441**, 24 (2014).
[46] D. J. Eisenstein and W. Hu, Power spectra for cold dark matter and its variants, Astrophys. J. **511**, 5 (1999).
[47] D. J. Eisenstein and W. Hu, Baryonic features in the matter transfer function, Astrophys. J. **496**, 605 (1998).
[48] E. Di Dio, F. Montanari, J. Lesgourgues, and R. Durrer, The CLASSgal code for relativistic cosmological large scale structure, J. Cosmol. Astropart. Phys. 11 (2013) 044.
[49] A. Lewis, A. Challinor, and A. Lasenby, Efficient computation of CMB anisotropies in closed FRW models, Astrophys. J. **538**, 473 (2000).
[50] C. Bonvin, R. Durrer, N. Khosravi, M. Kunz, and I. Sawicki, Redshift-space distortions from vector perturbations, J. Cosmol. Astropart. Phys. 02 (2018) 028.
[51] P. Bull, Extending cosmological tests of general relativity with the square kilometre array, Astrophys. J. **817**, 26 (2016).